Aspects of Geneva photometry : Part 4 : working with dusty data

Autor(en): **Cramer, Noël**

Objekttyp: **Article**

Zeitschrift: **Orion : Zeitschrift der Schweizerischen Astronomischen Gesellschaft**

Band (Jahr): **63 (2005)**

Heft 327

Aspects of Geneva Photometry[1]

Part 4 – Working with dusty data

NOËL CRAMER

In this fourth part of the article, we look at the manner in which interstellar extinction complicates the photometric calibration process even though the parameters used here are essentially reddening-free. This is particularly true for the fundamental observational estimate of stellar intrinsic luminosity habitually expressed as the absolute magnitude Mv. The primary stellar distance scale is based on trigonometrically derived distances (parallaxes) which are not affected by extinction. But, in the presence of interstellar reddening, one must be able to accurately compensate for that effect to fully exploit the distance data.

5.2.2. Using reddened primary data

The immediate solar neighbourhood is remarkably free of interstellar gas and dust. This is due to the fact that our sun is presently crossing a depleted region between interstellar clouds. If the local interstellar gas were to be compressed to the standard atmospheric pressure at sea level, the necessary «piston» would have to travel some 50 parsecs before that pressure is attained! This situation is expected to prevail for another hundred thousand years, more or less, when the solar system will finally catch up with the edge of the «local bubble» and again penetrate into denser media. However, as soon as observations are extended to objects significantly further than some 100 parsecs, interstellar extinction by dust becomes ever more present and has to be systematically taken into account in the interpretation of photometric measurements. The large scale distribution of interstellar matter is far from homogeneous (see Figs 46 and 47). The blasts of supernova explosions and the strong stellar winds of the most massive stars in young stellar associations play an important role in the structuring and dissemination of interstellar clouds.

Our whole perception of the cosmic distance scale relies critically on the knowledge of the trigonometrically determined distances of the stars in our closest neighbourhood. The first to successfully apply that method was KARL FRIEDRICH BESSEL in 1838 who estimated the distance of 61 Cyg with an error of only 27% relatively to the modern value. But, until the results of the HIPPARCOS Astrometric Satellite became publicly available in 1997, the number of distances thus measured was limited to less than 900 stars within 25 pc of the Sun. These stars are all of approximately solar mass, or less, except for a few cases such as Vega (A0 V) or Sirius (A1 V). Two notable exceptions to distances estimated by the direct parallax measurement were, in those days, the Hyades cluster in Taurus and the Scorpio-Centaurus association in the southern hemisphere, for which the «moving cluster» method could be applied. The rapid and well measurable apparent proper motions of their member stars and their obvious movement toward their respective convergence points in the sky provided geometric circumstances which allowed an independent evaluation of their distances to be made. The latter association, in particular, was the only group for which distances of the more massive «upper main sequence» B-type stars could be determined geometrically with satisfactory accuracy.

Now, the treatment of such fundamental and indisputable data as are the geometric distances – or parallaxes – of stars situated *beyond* 100 pc where interstellar extinction by dust is increasingly present is not at all straightforward. To be able to accede to the physical properties related with absolute luminosity via the absolute magnitude Mv, for example, one must be able to accurately de-redden the photometric measurements. Spectral classification is not influenced by relatively heavy extinction, and can provide such information in spite of it, but not with the same potential accuracy as photometry because of its discrete nature and lack of homogeneity (see Part 3 of this article). The nearby stars in the solar vicinity, however, are not significantly affected by extinction and the absolute magnitudes derived from their trigonometric parallaxes can be taken at face value. These Mv then serve to establish correlations such as spectral type versus absolute magnitude, or colour index versus absolute magnitude relations – i.e. the initial step in

Fig. 46. Looking toward the centre of our Galaxy, the irregularly shaped interstellar dust clouds clearly stand out – even to the naked eye – when viewed from the southern hemisphere as in this photograph taken from the ESO La Silla site in Chile (15 min. exposure with a 28 mm f:3.5 lens and 500 ASA emulsion). The more distant clouds form a narrow band that masks the central part of the galactic bulge in the background. The finely structured clouds that seem to depart from the galactic plane are in fact nearby features. The Upper Scorpius – Ophiuchus star forming region close to Antares (upper centre) is the younger part of the Scorpio-Centaurus stellar association and «only» at a distance of some 500 light years.

[1] Adapted from Archs Sci. Genève, Vol. 56, Fasc. 1, pp. 11-38, Juillet 2003. Based on data acquired at the La Silla (ESO, Chile), Jungfraujoch and Gornergrat (HFSJG International Foundation, Switzerland), and Haute-Provence (OHP, France) observatories.

the establishment of the HERTZSPRUNG – RUSSELL diagram (commonly referred to as the «H-R diagram»).

The pre-HIPPARCOS trigonometric parallaxes were comprehensively catalogued by WILHELM GLIESE and HARTMUT JAHREISS between 1969 and 1979. We show here the basic H-R diagram taken from GLIESE and JAHREISS (1979) in Fig. 48 for the stars within 25 pc having a standard error for Mv < 0.3 mag at the time of compilation of that list.

The magnitudes and distances of a star are linked by the following relation defining the «*apparent distance modulus*» $(m_v - M_v)$:

$$m_v - M_v = 5 \log_{10} r - 5 + A_v$$

Where $\mathbf{m_v}$ is the apparent visual magnitude, $\mathbf{M_v}$ the absolute magnitude, **r** the distance in parsecs and $\mathbf{A_v}$ the visual extinction (in the V band) in magnitudes. The latter is simply related to the colour excess:

$$A_v = R\, E_{[B-V]}$$

Where **R** is the «*ratio of total to selective visual absorption*». R depends on the locations of the bands used to derive the colour excess (B and V here) and, globally, to a lesser extent on the star's spectral energy distribution and the prevalent extinction law (see Fig 28, Part 2). In the Johnson U, B, V system its mean value lies between 3.0 and 3.2; and in the Geneva system its value for B-type stars is 2.75. The «*true apparent magnitude*» is:

$$m_{v0} = m_v - A_v$$

And $(m_{v0} - M_v)$ is then the «*true distance modulus*»

The consistent colour versus absolute magnitude diagram of Fig 48 can be constructed from *individual* stars because each of their distances is known and the interstellar reddening A_v may be neglected in the immediate solar vicinity. Even though the determination of trigonometric parallaxes can be extended much further – as the HIPPARCOS satellite has presently achieved – interstellar extinction would then have to be determined precisely in each case to be able to extend the fundamental H-R diagram to higher luminosities. This can be done, but with low accuracy and confidence by using simple colour-colour diagrams, as shown in Part 2. However, the situation gets much better if one does the adjustments *collectively*, by using colour versus apparent magnitude sequences of star clusters, where all stars may be considered to be practically at the same distance and reddened by the same amount.

That is essentially how the full stellar absolute magnitude scale was initially constructed on the basis of the locally prevalent trigonometric distance scale extended to higher luminosities via multi-colour photometry of open clusters.

We shall not yet discuss the difficulties of the method here; they involve considerations of age, chemical abundance, cluster membership, incidence of binary stars, radial extension of the cluster, variable extinction in the foreground, different values of the R ratio, etc. We shall simply give an illustration of the manner in which the photometric sequences of a number of open clusters can be adjusted to form the basic H-R diagram.

Fig. 47. The galactic centre is more difficult to observe from northern latitudes and the Milky Way less spectacular than in the South. Nevertheless, the equatorially situated Orion complex, one of the finest star forming regions in the sky, is prominent in winter as seen in this image taken from the Jungfraujoch Sphinx Observatory with the Jungfrau in the foreground. It is situated at roughly 1500 light years (three times the distance of the Upper Scorpius association) and one notes the apparently greater transparency of the interstellar medium in that direction (10 min. exposure with a 28 mm f:2.0 lens and 400 ASA emulsion).

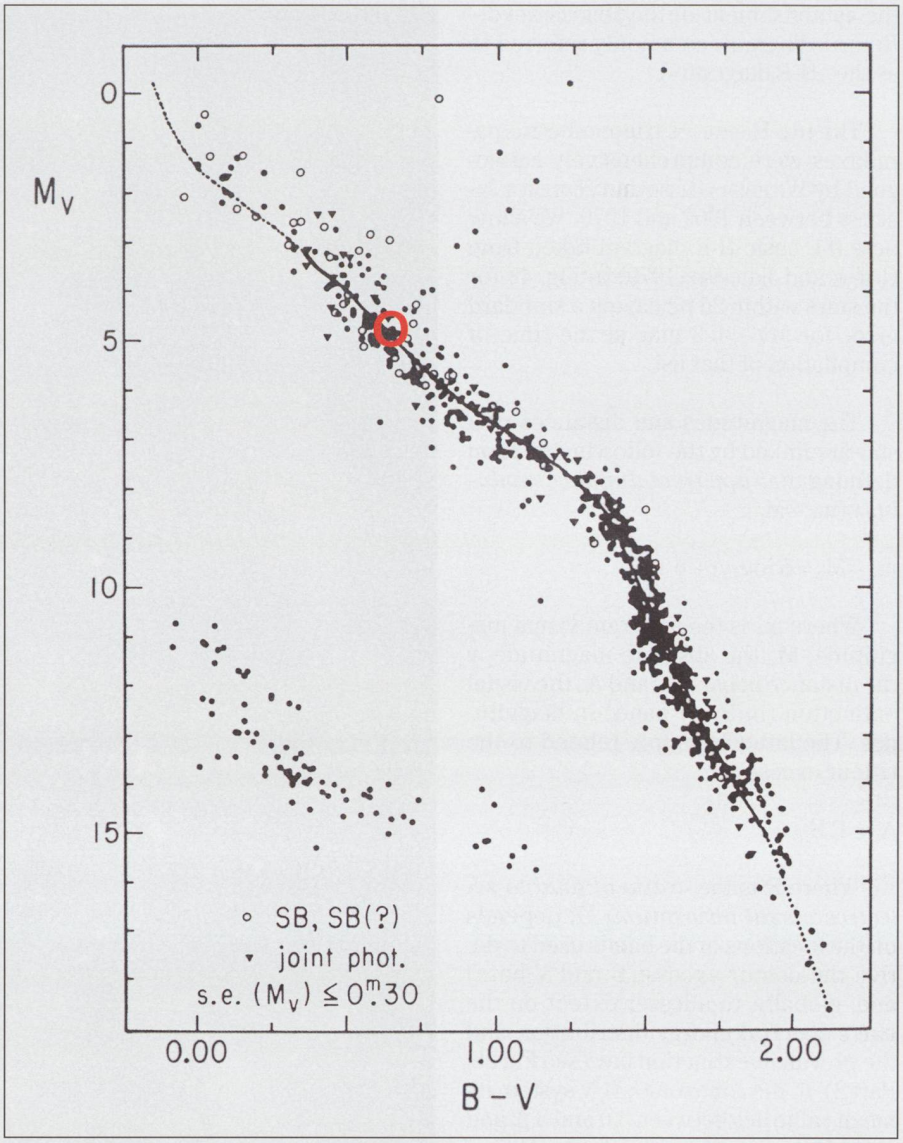

Fig. 48. H-R diagram of the stars within 25 pc (adapted from GLIESE and JAHREISS, 1979) having a standard error for Mv < 0.3 mag.. The yellow circle indicates the position the Sun would occupy in the «main sequence» of this diagram. The HIPPARCOS satellite has since considerably extended this sample. Note the «white dwarfs» at the lower left. These are older stars of initial mass smaller than 9M⊙ and that, after having lost much of their mass during their «red giant» phase, are in their final «degenerate» evolutionary stage following the termination of thermonuclear processes in their core. They are slowly drifting toward the right along their sequence as they cool down. A few stars can be seen just below the main sequence and running parallel to it. They belong to the «sub-dwarf» population of very old stars that appear bluer due to the lack of the «greenhouse effect» that the greater abundance of heavy elements causes in the atmospheres of our more contemporary neighbours.

In Fig. 49, we have considered 16 open clusters studied by W. BECKER (1963) which have also been measured in the Geneva system.

– In part 49***a***, we have plotted the «raw» measurements; i.e. the Geneva [V-B] index vs. the apparent magnitude m_v. Note that we have used [V-B] as it appears conventionally in the Geneva catalogue instead of [B-V]. Note also that the scales between the Johnson index (Fig. 48) and the Geneva one (Fig. 49) are different.

Fig. 49. Construction of the absolute H-R diagram based on the best measured trigonometric parallaxes of nearby stars (Fig. 48) serving to adjust a set of cluster sequences (before the HIPPARCOS satellite).

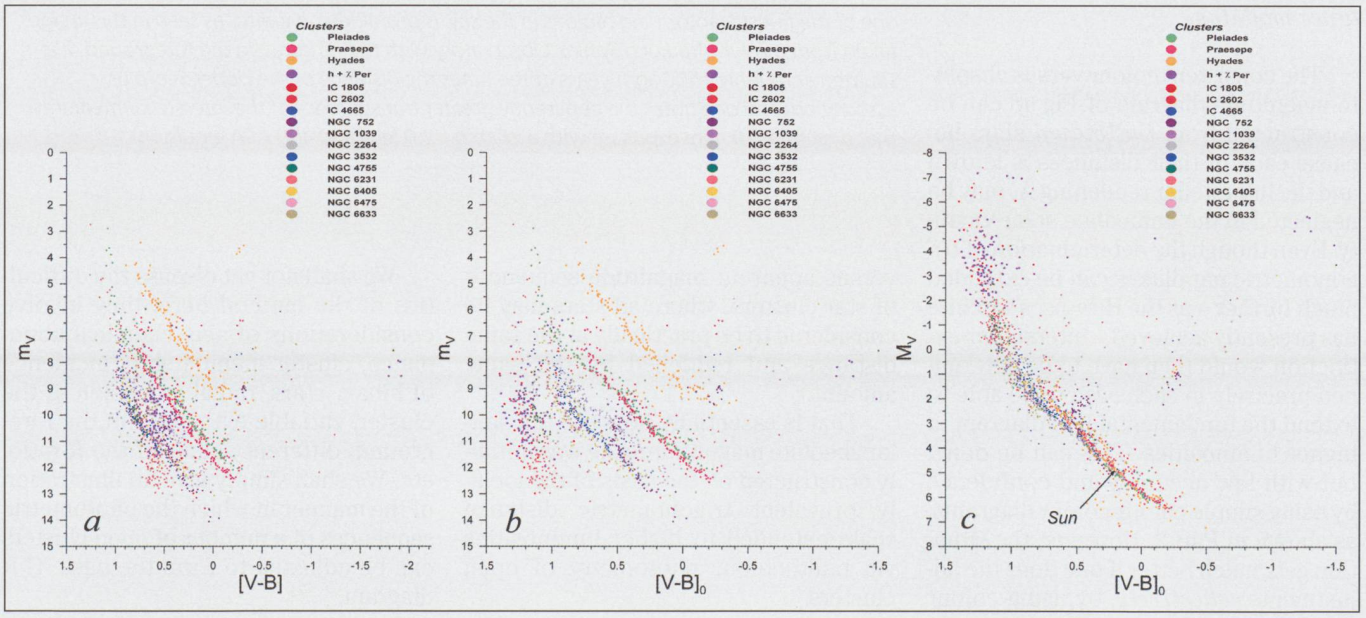

- In part 49***b***, these sequences are dereddened. As mentioned above, this is easier achieved when done *collectively* with a cluster sequence than for single stars. We have used the colour excess estimated by BECKER converted to the Geneva system to derive $[V\text{-}B]_0$.

- In part 49***c***, the sequence of Fig. 48 serves to merge the sequences of the nearest clusters in part 49***b*** that overlap by vertical translation to its fundamental distance (absolute magnitude) scale. These, in their turn, extend the scale to more distant clusters having overlapping sequences - and so on.

The composite sequence in part 49***c*** uses the distance moduli ($m_v - M_v$) and the extinctions A_v estimated by BECKER. Most of these nearby clusters already show the effects of stellar evolution with the presence of «*red giants*» to the right of the main sequence. One also notices the effect of cluster age. Evolution is much more rapid for massive stars. A photometric cluster H-R diagram starting out as the composite sequence in Fig 49***c*** would progressively be depleted from the top downwards as its members evolve to red giants. The point where this departure from the main sequence occurs is the «*turnoff point*» which is narrowly related to the cluster's age. In the latter figure the oldest cluster is NGC 752 with an age of about 1.1 10^9 years. The interpretation of cluster H-R diagrams in terms of stellar evolution is a whole subject by itself and will not yet be discussed here, since our current object is the empirical calibration of the (X, Y) parameters in terms of absolute magnitude.

5.2.2.1. The absolute magnitude problem. Second to that of intrinsic colours

As seen above, the procedure leading to Fig 49***c*** can be extended to a large number of open clusters and produce an even larger number of values of M_v liable to calibrate in a straightforward manner – i.e. without having to correct further for extinction – a reddening-free parameter diagram such as (X, Y). The quality of the data, however, will depend merely on that of the extrapolation from the relatively limited sample of Fig 48 and on the accuracy of the correction for reddening of each cluster.

A first calibration of the (X, Y) diagram in terms of absolute magnitudes was made for B-stars (CRAMER and MAEDER, 1979) on the basis, essentially, of cluster moduli derived by W. BECKER and R. FENKART in 1971. The accuracy of the resulting two-dimensional $M_v(X,Y)$ estimator was reasonably good with a standard deviation of 0.38 mag over some 200 calibration stars of luminosity classes V to III.

To progress further, however, and be able to use trigonometric parallax data for more distant single stars subject to interstellar extinction – such as those provided by the HIPPARCOS satellite – it is necessary to be able to compensate for reddening *individually* with a high degree of accuracy. That is particularly true for the B-stars, none of which is free of reddening. In other words, it is necessary to calibrate the reddening-free parameter space in terms of *intrinsic colours* so as to estimate precise colour excesses in each case by comparison with the observed colours.

So, the process of determining M_v by a photometric calibration, and the application of the latter to the determination of stellar distances, is linked to the accurate knowledge of the intrinsic colours. On the other hand, if accurate distances are known and are to serve in refining an M_v calibration, intrinsic colours must absolutely be well defined. But the establishment of an *unprejudiced* intrinsic colour calibration depends on the knowledge of M_v since an *extrapolation* is necessary in the case of this universally reddened population of stars, as will be shown below. The circumstances are somewhat circular but can be solved empirically by a succession of converging processes.

Fig. 50: Selection of a given group of «quasi identical» stars (red crosses in the yellow field) in the reddening-free (X, Y) diagram with their corresponding locations in the [U, B, V] diagram to the right. The blue line to the right is a first approximation of a limiting reference locus relatively to which the true zero point $[U, B, V]_0$ of each group may be estimated (see Fig 51).

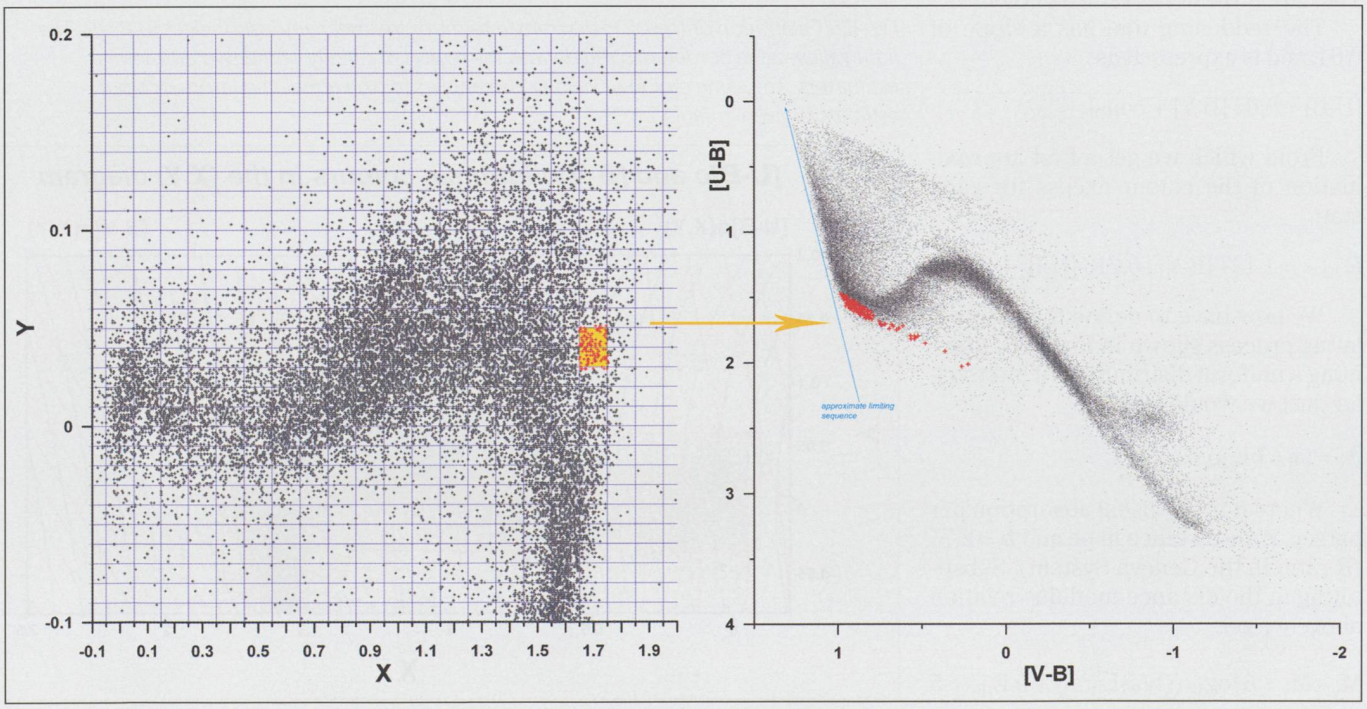

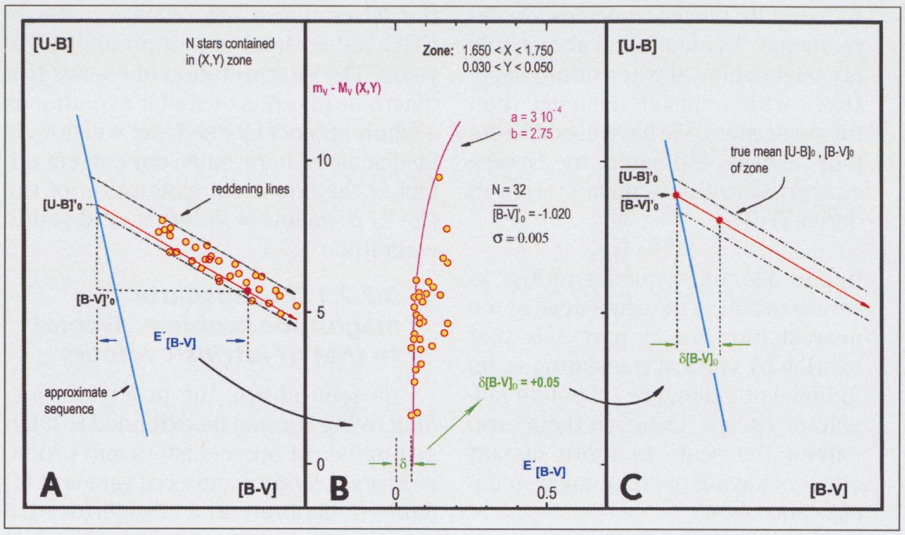

Fig. 51: Determination of the mean intrinsic $[U,B,V]_0$ indices of the zone selected in fig 50. Part A reflects the situation shown in Fig 50, right. Part B makes use of the first $M_v(X,Y)$ calibration to determine a satisfactory value of the apparent distance modulus of each star. This is plotted as a function of the approximate colour index E'[B-V] taken relatively to the arbitrary limiting line. The extrapolation to the point of zero extinction is done with the «blue envelope» reddening line assuming a minimum diffuse extinction of $a = 3\ 10^{-4}$ [mag pc^{-1}]. The value b = 2.75 is the R ratio in the Geneva system. Part C shows the true mean intrinsic colours of the selected zone in the (X,Y) diagram after correction of E'[B-V] by the difference $\delta[B-V]_0$.

Doing the work «by hand»

The first step in that direction was done by establishing the Mv(X,Y) calibration mentioned above. The second is the calibration of the X, Y plane in terms of the intrinsic Geneva [U, B, V] indices.

Without going into details, the method is shown in Figures 50 and 51:

A group of stars in a small zone of the (X,Y) diagram is selected. These may be considered to be quasi identical (Fig. 50). Their positions in the reddening-prone [U,B,V] diagram are shown at the right of the figure.

The situation in Fig. 50, right, is shown in detail in Fig 51A. The approximate limiting sequence was taken as:

$$[U-B]'_0 = 5.328\ [B-V]'_0 + 6.923$$

These are *not* the intrinsic indices. They are provisional values of them.

The reddening line has a slope of 0.64, and is expressed as:

$$[U-B] = 0.64\ [B-V] + \text{const.}$$

From which we get a first approximation of the colour excess for each star:

$$E'_{[B-V]} = 1.137\ [B-V] - 0.213\ [U-B] + 1.477$$

We now have to define the extrapolating process shown in Fig. 51B. Assuming a uniform distribution of interstellar dust we would have:

$$A_v = ar = bE_{[B-V]}$$

Where $\boldsymbol{a}$ is the visual absorption per parsec, $\boldsymbol{r}$ the distance in pc and $\boldsymbol{b}$ = 2.75 (R ratio in the Geneva System). Substituting in the distance modulus relation above we get:

$$M_v - M_v = 5 \log_{10}((b/a)E_{[B-V]}) + b\ E_{[B-V]} - 5$$

Which gives the *shape* of the corresponding reddening line in Fig. 51B. Its «shaping factor» is essentially determined here by the value of $\boldsymbol{a}$. Now, the interstellar medium is far from being uniform. But, if we examine in detail all the relevant similar zones in the (X,Y) diagram, the blue envelopes of the corresponding $(m_v - M_v(X,Y))$ versus $E'_{[B-V]}$ figures are consistently represented by a minimum, diffuse interstellar extinction of $a = 3\ 10^{-4}$ mag pc^{-1}.

The difference between the approximate excess $E'_{[B-V]}$ and the asymptotic value of the thus defined reddening line fitted by translation as a blue envelope gives the correction $\delta[B-V]_0$. The (X,Y) plane was calibrated in this manner point by point over the domain covered by the O, B and first A-type stars of classes V to III. Two third degree polynomials in X and Y were then fitted as global estimators of the intrinsic $[U-B]_0$ and $[B-V]_0$ indices (CRAMER, 1982). These two relations are shown in Fig. 52.

The importance, and *originality*, of these estimators is the fact that they are two-dimensional. They are physically related to the evolutionary stage of each star through their combined sensitivity to temperature and surface gravity. In contrast to other photometric systems, just one relation is needed to estimate the colour excess regardless of prior knowledge of the star's evolutionary status.

For all practical purposes involving the determination of the absolute magnitude M_v only the intrinsic $[B-V]_0$ is needed to evaluate the colour excess $E_{[B-V]}$:

Fig. 52: Calibration of the (X,Y) diagram in terms of the mean intrinsic indices $[U,B,V]_0$. The light yellow zone bordered in red defines the region of validity of the two polynomial estimators. The same region of validity also applies for the remaining intrinsic colour estimators given in Table 2.

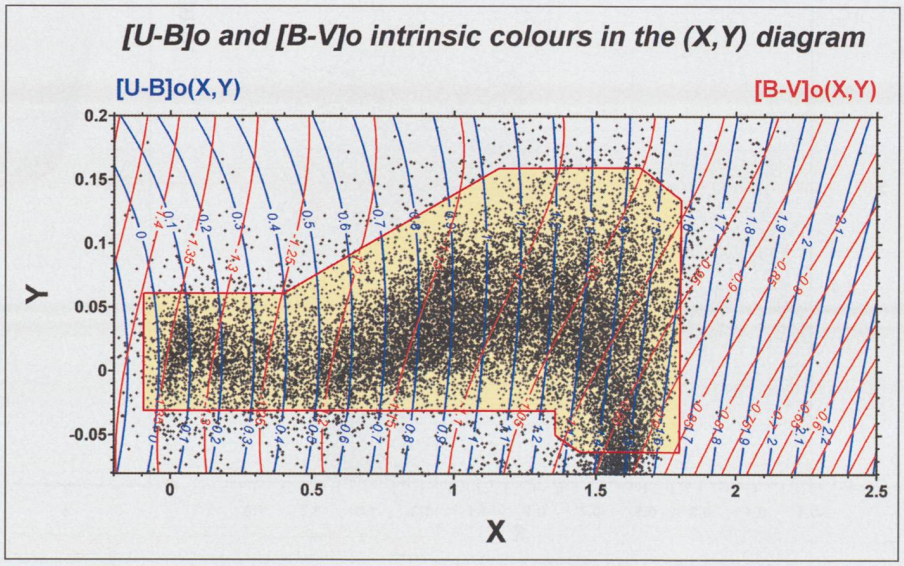

$[k\text{-}B]_o(X,Y) = a_0 + a_1X + a_2Y + a_3XY + a_4X^2 + a_5Y^2 + a_6XY^2 + a_7X^2Y + a_8X^3 + a_9Y^3$ *where k = U-B, V-B, B1-B, B2-B, V1-B, G-B*

Index	a_0	a_1	a_2	a_3	a_4	a_5	a_6	a_7	a_8	a_9
[U-B]	0.0380	0.9057	-0.0625	-0.2409	-0.0518	4.8627	-2.6551	-0.0340	0.0240	1.9123
[V-B]	1.3431	-0.3227	0.2400	-0.3371	0.1582	1.6294	-1.1422	0.4078	-0.0638	-5.4104
[B1-B]	0.7413	0.0937	-0.2001	-0.0480	-0.0152	1.0014	-0.5845	-0.0249	0.0067	1.6738
[B2-B]	1.6408	-0.0878	0.2403	0.0721	0.0061	-2.3129	1.2373	-0.0151	-0.0039	1.6564
[V1-B]	2.0062	-0.2480	0.0974	0.4180	0.0752	-6.2176	3.1873	-0.0139	-0.0350	0.8075
[G-B]	2.5758	-0.2907	0.0734	0.4734	0.0823	-9.9578	5.3204	0.0013	-0.0398	1.1033

Table 2: Coefficients of the Geneva intrinsic colour estimators $[k\text{-}B]_0(X,Y)$ for B-type stars.

$E_{[B-V]} = [B-V] - [B-V]_0(X,Y)$

However, having thus obtained the estimators of these two basic intrinsic colour indices of the [U,B,V] plane, it is relatively easy to derive similar ones for the remaining Geneva normalised indices B1, B2, V1 and G (these are actually [B1-B], [B2-B], [V1-B] and [G-B], as defined in Part 2).

Now, the X, Y and Z parameters are linear combinations of the five indices U, B1, B2, V1 and G. The first one of these, U, has known intrinsic values (given by $[U-B]_o(X,Y)$), so we have three equations (X, Y and Z) with four unknowns. To get rid of one of the latter, the [B2-B] index is first tied to the zero points of the $[B-V]_0(X,Y)$ and $[U-B]_o(X,Y)$ calibrations by correlation for about 160 zones in the X, Y plane, thus defining an equal number of $[B2-B]_0$ intrinsic values (see CRAMER, 1993). The respective mean values of X and Y define each of these zones. By its nature, the true mean value of Z is very small throughout, but not strictly zero, and depends on the physical properties of the stars present in the given zone as well as on small residual effects of reddening. So, its mean zero point Z_0 is determined for each zone by regression of its observed values over the estimated visual colour excess A_v (CRAMER, 1993).

We now have some 160 sets of three equations (X, Y, Z_0) as linear functions of the three unknowns $[B1-B]_0$, $[V1-B]_0$ and $[G-B]_0$. Solving these systems and fitting cubic surface polynomials to each of the four remaining sets of intrinsic colours, we finally get the basic intrinsic colour calibration for B-type stars in the Geneva system shown in Table 2. Their validity region is that of Fig. 52, and their properties regarding evolutionary stage, as mentioned above, are the same throughout.

Note that we have listed the estimator for [V-B] in Table 2 for reasons of consistency with the other indices. If one prefers to use the [B-V] index, one just has to change the signs.

The knowledge of the intrinsic colours enables us to determine the colour excess ratios between various colour indices in a straightforward manner by simple correlation. These ratios are particularly important when one studies reddened stellar clusters by means of a multicolour photometry. That is because the colour excesses estimated via different colour combinations have then to be consistent with one another. The colour excess ratios also lie at the source of the description of the extinction law by interstellar dust (see Fig. 28, Part 2). All the colour excess ratio combinations of the Geneva system relative to the $E_{[B-V]}$ excess derived in this manner with the aid of our calibrations based on B-type stars are listed in table 3. The [B-V] excess was chosen as a common denominator since it is the most often used in the astronomical literature.

Finally, we may apply these calibrations to determine the intrinsic Geneva colours of the MK spectral types as given in Table 4. We have omitted the repetition of the (X,Y) values of Table 1, Part 3, but have added the often used indices $[B1-B2]_o$, $[U-B2]_o$, $[B2-V1]_o$ and $[V1-G]_o$.

Table 3: Colour excess ratios relative to [B-V]

Colour	$E_{[Colour]}/E_{[B-V]}$	σ(ratio)
U-B	0.654	0.003
B1-B	0.158	0.002
B2-B	-0.195	0.002
V1-B	-0.943	0.002
G-B	-1.208	0.003
U-B1	0.497	0.001
B1-B2	0.351	0.001
B2-V1	0.750	0.002
V1-G	0.266	0.003
U-B2	0.848	0.003
B2-G	1.014	0.003
U-V1	1.597	0.004
U-G	1.861	0.005
U-V	1.654	0.003
B1-V1	1.100	0.003
B1-G	1.364	0.004
B1-V	1.157	0.002
V1-V	0.062	0.002
G-V	-0.210	0.003
B2-V	0.807	0.002

Why not just use theoretical stellar atmosphere models?

It has been mentioned earlier (Part 3) that good theoretical stellar radiative spectral energy distributions can be filtered by the passbands of a multicolour photometry. Ideally, such «synthetic photometry» would render empirical calibrations similar to those presented here unnecessary. But as pointed out earlier, particularly in the context of the effective temperature calibration, synthetic photometry relies on a series of processes, each of which is subject to some potential source of error. We shall illustrate the point by means of KURUCZ's (1993) solar composition models filtered by the passbands defined by RUFENER and NICOLET (1988).

A direct comparison can be made by using real observations. For the sake of clarity, the comparison is made in the familiar [U,B,V] diagram. The stars selected have measurements weighted P≥ 3, and are chosen among the least reddened ones of classes V to III ($E_{[B-V]} \leq 0.08$ for $X \leq 0.6$ and $E_{[B-V]} \leq 0.12$ for $X < 0.6$). The result is shown in figs 53**a,b,c**:

- In fig. 53**a**, the overall aspect of the selected stars superimposed on the synthetic lines of the models with log g ranging from 5 to 3.5 does not, at first glance, give an impression of significant discord. This comparison would even be considered as quite satisfactory if it were not recognized that the B-stars are *systematically* reddened. A few stars do, however, trespass the log g = 3.5 line and may give the impression of being somewhat too blue.

- If the individual stars are de-reddened by the estimators, as in fig. 53**b**, the observed sequence narrows down and becomes decidedly bluer than that of the models. The cut-off

Class V	$[U-B]_o$	$[B-V]_o$	$[B1-B]_o$	$[B2-B]_o$	$[V1-B]_o$	$[G-B]_o$	$[B1-B2]_o$	$[U-B2]_o$	$[B2-V1]_o$	$[V1-G]_o$
O6	0.029	-1.349	0.739	1.644	2.009	2.578	-0.905	-1.614	-0.365	-0.569
O7	0.032	-1.348	0.739	1.644	2.008	2.577	-0.905	-1.611	-0.364	-0.569
O8	0.035	-1.347	0.739	1.644	2.007	2.576	-0.905	-1.609	-0.364	-0.569
O9V	0.069	-1.336	0.742	1.641	1.998	2.565	-0.899	-1.572	-0.357	-0.567
O9.5V	0.103	-1.325	0.745	1.638	1.989	2.554	-0.894	-1.535	-0.351	-0.565
B0V	0.131	-1.316	0.747	1.636	1.982	2.545	-0.889	-1.505	-0.346	-0.563
B0.5V	0.210	-1.290	0.755	1.628	1.962	2.523	-0.873	-1.418	-0.334	-0.560
B1V	0.269	-1.272	0.762	1.622	1.948	2.506	-0.860	-1.353	-0.326	-0.558
B1.5V	0.325	-1.255	0.768	1.615	1.934	2.490	-0.847	-1.290	-0.319	-0.556
B2V	0.452	-1.221	0.782	1.601	1.904	2.454	-0.819	-1.149	-0.302	-0.551
B2.5V	0.521	-1.203	0.789	1.594	1.887	2.435	-0.804	-1.072	-0.293	-0.548
B3V	0.576	-1.191	0.794	1.589	1.875	2.420	-0.794	-1.013	-0.287	-0.545
B4V	0.645	-1.175	0.801	1.582	1.860	2.402	-0.782	-0.937	-0.278	-0.542
B5V	0.702	-1.163	0.805	1.578	1.849	2.388	-0.773	-0.876	-0.271	-0.539
B6V	0.805	-1.143	0.813	1.570	1.829	2.363	-0.757	-0.765	-0.259	-0.534
B7V	0.849	-1.134	0.816	1.567	1.821	2.353	-0.751	-0.718	-0.254	-0.532
B8V	1.016	-1.106	0.826	1.556	1.791	2.315	-0.730	-0.540	-0.236	-0.524
B8.5V	1.091	-1.091	0.831	1.549	1.776	2.296	-0.718	-0.459	-0.227	-0.520
B9V	1.256	-1.051	0.848	1.532	1.736	2.249	-0.684	-0.276	-0.204	-0.513
B9.5V	1.339	-1.023	0.859	1.521	1.709	2.217	-0.662	-0.182	-0.188	-0.508
A0V	1.407	-0.991	0.872	1.508	1.678	2.182	-0.636	-0.101	-0.171	-0.503
A1V	1.457	-0.960	0.885	1.495	1.648	2.146	-0.610	-0.038	-0.153	-0.498
A2V	1.494	-0.929	0.898	1.482	1.616	2.109	-0.584	0.012	-0.134	-0.493
A3V	1.501	-0.915	0.905	1.475	1.599	2.089	-0.570	0.027	-0.124	-0.490
Class IV	**$[U-B]_o$**	**$[B-V]_o$**	**$[B1-B]_o$**	**$[B2-B]_o$**	**$[V1-B]_o$**	**$[G-B]_o$**	**$[B1-B2]_o$**	**$[U-B2]_o$**	**$[B2-V1]_o$**	**$[V1-G]_o$**
O9IV	0.037	-1.346	0.739	1.643	2.007	2.576	-0.904	-1.606	-0.364	-0.569
O9.5IV	0.087	-1.328	0.744	1.638	1.993	2.560	-0.894	-1.551	-0.355	-0.567
B0IV	0.121	-1.317	0.748	1.635	1.985	2.550	-0.888	-1.515	-0.349	-0.565
B0.5IV	0.161	-1.304	0.752	1.632	1.975	2.538	-0.880	-1.471	-0.343	-0.563
B1IV	0.242	-1.279	0.760	1.624	1.954	2.514	-0.864	-1.381	-0.331	-0.560
B1.5IV	0.287	-1.266	0.764	1.619	1.943	2.501	-0.855	-1.332	-0.324	-0.558
B2IV	0.354	-1.247	0.771	1.613	1.928	2.483	-0.842	-1.258	-0.315	-0.555
B2.5IV	0.496	-1.211	0.785	1.599	1.896	2.444	-0.814	-1.102	-0.297	-0.548
B3IV	0.613	-1.185	0.794	1.589	1.871	2.414	-0.795	-0.976	-0.282	-0.543
B4IV	0.659	-1.175	0.798	1.585	1.862	2.403	-0.788	-0.926	-0.277	-0.541
B5IV	0.694	-1.169	0.800	1.583	1.855	2.394	-0.783	-0.889	-0.272	-0.539
B6IV	0.820	-1.146	0.808	1.574	1.832	2.364	-0.765	-0.754	-0.258	-0.532
B7IV	0.870	-1.138	0.811	1.571	1.823	2.352	-0.759	-0.701	-0.252	-0.529
B8IV	0.957	-1.122	0.818	1.564	1.806	2.331	-0.746	-0.607	-0.243	-0.525
B9IV	1.172	-1.079	0.835	1.545	1.763	2.279	-0.709	-0.373	-0.218	-0.516
B9.5IV	1.319	-1.038	0.852	1.527	1.723	2.233	-0.676	-0.208	-0.196	-0.510
A0IV	1.403	-1.006	0.864	1.515	1.693	2.198	-0.650	-0.112	-0.178	-0.505
A1IV	1.505	-0.937	0.893	1.488	1.627	2.122	-0.595	0.017	-0.140	-0.495
A2IV	1.509	-0.914	0.904	1.475	1.600	2.090	-0.571	0.034	-0.124	-0.490
Class III	**$[U-B]_o$**	**$[B-V]_o$**	**$[B1-B]_o$**	**$[B2-B]_o$**	**$[V1-B]_o$**	**$[G-B]_o$**	**$[B1-B2]_o$**	**$[U-B2]_o$**	**$[B2-V1]_o$**	**$[V1-G]_o$**
O9III	0.058	-1.340	0.741	1.642	2.001	2.569	-0.901	-1.584	-0.359	-0.567
O9.5III	0.075	-1.334	0.742	1.641	1.997	2.563	-0.898	-1.566	-0.356	-0.567
B0III	0.078	-1.334	0.742	1.640	1.996	2.562	-0.898	-1.563	-0.355	-0.566
B0.5III	0.152	-1.310	0.749	1.634	1.977	2.539	-0.885	-1.483	-0.342	-0.562
B1III	0.218	-1.289	0.755	1.628	1.960	2.520	-0.873	-1.410	-0.332	-0.559
B1.5III	0.290	-1.267	0.763	1.621	1.943	2.500	-0.858	-1.330	-0.322	-0.556
B2III	0.326	-1.257	0.766	1.617	1.935	2.490	-0.851	-1.292	-0.318	-0.555
B3III	0.563	-1.197	0.789	1.594	1.882	2.427	-0.805	-1.031	-0.288	-0.545
B4III	0.646	-1.178	0.797	1.586	1.864	2.406	-0.789	-0.940	-0.278	-0.541
B5III	0.767	-1.155	0.805	1.577	1.841	2.376	-0.772	-0.810	-0.264	-0.535
B6III	0.830	-1.144	0.809	1.573	1.830	2.361	-0.764	-0.743	-0.257	-0.531
B7III	0.855	-1.141	0.810	1.572	1.826	2.356	-0.762	-0.717	-0.254	-0.530
B8III	0.952	-1.127	0.815	1.566	1.810	2.333	-0.752	-0.615	-0.243	-0.524
B9III	1.124	-1.100	0.825	1.555	1.780	2.295	-0.730	-0.431	-0.225	-0.515
B9.5III	1.216	-1.083	0.831	1.548	1.764	2.276	-0.717	-0.332	-0.215	-0.512
A0III	1.366	-1.046	0.846	1.533	1.729	2.237	-0.687	-0.166	-0.196	-0.508
A1III	1.489	-0.984	0.871	1.507	1.672	2.172	-0.636	-0.018	-0.164	-0.501
A2III	1.516	-0.933	0.894	1.486	1.624	2.118	-0.593	0.030	-0.138	-0.494
A3III	1.506	-0.912	0.906	1.473	1.595	2.085	-0.567	0.033	-0.122	-0.490

Table 4: MK-Type versus intrinsic colour correlation

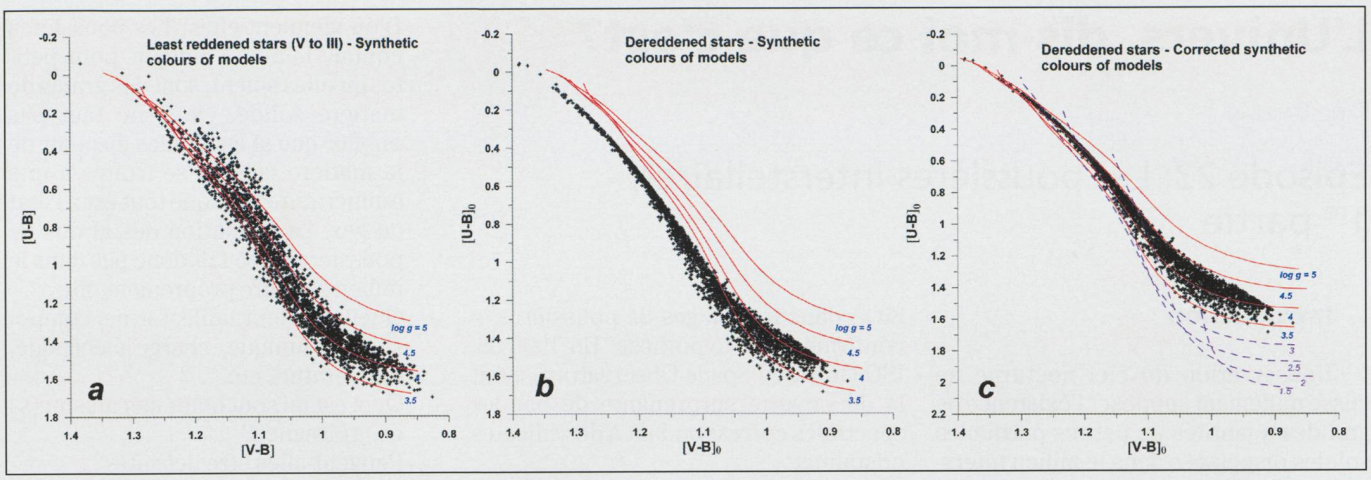

*Fig. 53: Fig. 53**a** Synthetic Geneva [U,B,V] colours of Kurucz's models with log g = 3.5, 4.0, 4.5, 5.0 compared with the least reddened well measured O, B and first A stars of classes V to III in the Geneva catalogue. Fig. 53**b**. Same comments as for fig. 53**a**, but with the stars de-reddened by the intrinsic colour estimators. The estimated intrinsic sequence is definitely bluer than the synthetic locus. Fig. 53**c**. Synthetic colours shifted by -0.035 mag in [U-B] and 0.050 mag in [V-B]. The fit is excellent throughout the whole sequence. The equally shifted lines of lower gravity (in violet) have been added in this figure to illustrate the ambiguity inherent to the de-reddening of supergiants.*

at the bottom right of the stellar sequence reflects the cut-off at Y = –0.06 to discard stars that lie outside the field of definition of the intrinsic colour estimators (Fig. 52).

– If we apply simple corrections to the models (–0.035 and +0.050, respectively) we get the very satisfactory situation seen in fig. 53**c**. The upper envelope (higher g, class V) of the empirical sequence follows the log g = 4.5 line throughout its length. The top of the sequence favours a somewhat higher gravity whereas the bottom tends to drift towards lower log g. This is in good agreement with predictions of stellar internal structure models. The shape of the lower envelope (class III) is also well fitted by the log g = 4 and 3.5 lines. These results validate the use we made of the synthetic relation's «shape» while calibrating T_{eff} and B.C. in Part 3. We have included the predictions for lower gravities in this last figure. They serve to illustrate the difficulty of de-reddening supergiants.

This topic is discussed in greater detail (in CRAMER, 1999) and the conclusion is that the main body of the discrepancy must reside in the combination of the small uncertainties over the model flux distributions with those inherent to the definition of the passbands. The latter is achieved through an elaborate process that depends closely on the quality of external spectrophotometric data that have also to be de-reddened before being applied.

The next part of this article will extensively exploit the intrinsic colour calibrations and more particularly examine the calibration of absolute magnitudes using data acquired by the HIPPARCOS satellite.

NOËL CRAMER
Observatoire de Genève
Chemin des Maillettes 51, CH-1290 Sauverny

Bibliography 4:

BECKER, W.: 1963, *Die räumliche Verteilung von 156 galaktischen Sternhaufen in Abhängigkeit von ihrem Alter*, Mitteil. Astron. Meteor. Anstalt Uni. Basel, **28**, 117

BECKER, W., FENKART, R.P.: 1971, *A Catalogue of Galactic Star Clusters observed in three colours,* A&A Suppl. **4**, 241

CRAMER, N., MAEDER, A.:1979, *Luminosity and T_{eff} determinations for B-type stars*, A&A **78**,305

CRAMER, N.:1982, *Geneva [U,B,V] Intrinsic Colours of B-type Stars*, A&A **112**, 330

CRAMER, N.: 1993, *Intrinsic colours of O, B and early A-type stars in the Geneva system*, A&A **269**, 457

CRAMER, N.: 1999, Calibrations *for B-type stars in the Geneva photometric system*, review article, New AR **43**, 343

GLIESE, W, JAHREISS, H.:1979, Nearby star data published 1969 – 1978, A&A Suppl. **38**, 423

KURUCZ, R.L.: 1993, Kurucz CD-ROM 13, *ATLAS9 stellar atmosphere program and 2 km/s grid*

RUFENER, F., NICOLET, B.: 1988, *A new determination of the Geneva photometric passbands and their absolute calibration*, A&A **206**, 357